NANO LETTERS

2007
Vol. 7, No. 6
1649−1654

Determination of Transport Properties in Chromium Disilicide Nanowires via Combined Thermoelectric and Structural Characterizations

Feng Zhou,[†] Jeannine Szczech,[‡] Michael T. Pettes,[§] Arden L. Moore,[§] Song Jin,[‡] and Li Shi*[,†,§,||]

Materials Science and Engineering Program, Texas Materials Institute, The University of Texas at Austin, Austin, Texas 78712, Department of Chemistry, University of Wisconsin—Madison, Madison, Wisconsin 53706, Department of Mechanical Engineering, The University of Texas at Austin, Austin, Texas 78712, and Center for Nano and Molecular Science and Technology, The University of Texas at Austin, Austin, Texas 78712

Received March 14, 2007; Revised Manuscript Received April 30, 2007

ABSTRACT

The Seebeck coefficient, electrical conductivity, and thermal conductivity of individual chromium disilicide nanowires were characterized using a suspended microdevice and correlated with the crystal structure and growth direction obtained by transmission electron microscopy on the same nanowires. The obtained thermoelectric figure of merit of the nanowires was comparable to the bulk values. We show that combined Seebeck coefficient and electrical conductivity measurements provide an effective approach to probing the Fermi Level, carrier concentration and mobility in nanowires.

The energy efficiency of thermoelectric (TE) devices is limited by the TE figure of merit *ZT*, which is defined as $ZT \equiv S^2\sigma T/\kappa$, where S is the Seebeck coefficient, σ is the electrical conductivity, and κ is the thermal conductivity consisting of a phonon or lattice contribution (κ_l) and an electron contribution (κ_e). It has been predicted that *ZT* can be enhanced in nanostructured materials because of classical and quantum confinement effects on electron and phonon transport. Guided by such theoretical predictions, enhanced *ZT* has been demonstrated in thin film supperlattices[1,2] and bulk nanocomposites,[3] although the *ZT* increase was mainly attributed to κ_l reduction and the contribution of the quantum confinement has not been verified experimentally in two-dimensional (2D) quantum wells and one-dimensional (1D) nanowires (NWs).

The progress in the research of NW structures for TE applications has been hindered by the crystal quality of the NWs and the difficulty in measuring the TE properties of NWs. In particular, the TE properties of a NW depend critically on the crystal structure including crystallinity, growth direction, surface roughness, and defects. However, conducting TE property measurement and crystal structure analysis on the same individual NW has not been demonstrated to date. In addition, the Fermi Level (E_F), carrier concentration, and mobility in NWs are fundamental parameters that are critical for optimizing the *ZT* values. Efforts have been made to obtain the E_F or carrier concentration in NWs using Shubnikov−de Hass (SdH) effects[4] or from electrical conductivity measurements.[5,6] However, the SdH method is experimentally complex and not applicable for heavily dope NWs, whereas TE materials often need to be degenerately doped in order to maximize the power factor. In addition, electrical conductivity alone is insufficient to determine these charge transport parameters.

In this Letter, we report an experimental approach to characterize the TE properties of single-crystal chromium disilicide ($CrSi_2$) NWs and correlate them with the crystal structure of the same NWs. We show that the E_F, carrier concentration, and mobility of the NWs can be obtained from its temperature-dependent Seebeck coefficient and electrical conductivity. The as-obtained results will provide guidelines for optimizing the *ZT* of NW structures.

$CrSi_2$ is one of the semiconducting silicides that have been investigated for TE applications.[7,8] Among these silicides, β-$FeSi_2$ with highest *ZT* about 0.4 was deployed in early

* Corresponding author. E-mail: lishi@mail.utexas.edu.
[†] Materials Science and Engineering Program, Texas Materials Institute, The University of Texas at Austin.
[‡] Department of Chemistry, University of Wisconsin—Madison.
[§] Department of Mechanical Engineering, The University of Texas at Austin.
[||] Center for Nano and Molecular Science and Technology, The University of Texas at Austin.

10.1021/nl0706143 CCC: $37.00
Published on Web 05/18/2007

NASA TE modules.[8] The most notable TE silicides are $MnSi_{1.8}$ with *ZT* values up to 0.7[8] and $ReSi_{1.8}$ with reported *ZT* up to 0.8,[9] both in the intermediate temperature range of 500−900 K. Many other narrow band gap semiconducting silicides including Mg_2Si and $CrSi_2$ have been explored as TE materials. Single-crystal free-standing NWs of metal silicides,[10−15] including those semiconducting silicides, have only become available recently due to the development of general synthetic methods using chemical vapor deposition of organometallic precursors[12,13] and chemical vapor transport (CVT).[14] The CVT method was employed to synthesize the $CrSi_2$ NWs.[15] $CrSi_2$ has an indirect band gap of 0.35 eV and a hexagonal *C*40 crystal structure.[16] This specific crystal structure leads to anisotropic TE properties along different directions, i.e., parallel or perpendicular to the *c*-axis, which have been observed experimentally in bulk $CrSi_2$ crystals.[17] Although the *ZT* of bulk $CrSi_2$ crystals was found to be low and high *ZT* is not expected for $CrSi_2$ NWs, the capability demonstrated here for the growth and combined TE−structure characterization of individual $CrSi_2$ NWs will enable us to employ the synthesis and characterization methods to further investigate NW structures of other silicides with high bulk *ZT* values.

We used a nanofabricated device shown in Figure 1a to characterize *S*, σ, κ, and *ZT* of individual $CrSi_2$ NWs. The device incorporated two adjacent silicon nitride (SiN_X) membranes each suspended with six SiN_X beams. One serpentine platinum resistance thermometer and two platinum electrodes were patterned on each membrane. There was a through-substrate hole in the substrate under the suspended membrane so that transmission electron microscopy (TEM) could be used to characterize the crystal structure of the same NW. This capability enables us to correlate the obtained TE properties with the anisotropic crystal structure especially the growth direction of $CrSi_2$ NWs.

An individual $CrSi_2$ NW was trapped between the two membranes of a device after NW suspensions in ethanol were dropped on a wafer piece containing eight devices. A total of three individual NW samples were investigated using three measurement devices similar to that shown in Figure 1. The native oxide on the NW surface prevents electrical contact between the NW and the four platinum electrodes pre-patterned on the two membranes. On each platinum electrode, a 1500 nm wide, 600 nm long, and 200 nm thick platinum pattern was deposited on the NW using a focused ion beam (FIB) deposition method (Figure 1b). The native oxide on the NW surface was damaged during the FIB deposition process, which resulted in ohmic contact to the NW. During the deposition process, care was taken to prevent ion damage or contamination of the NW except at the four contact areas.

The TE measurements were conducted according to the procedure described in refs 18−20. In addition to four-probe measurement of the electrical conductivity of all three NW samples, the Seebeck coefficient and thermal conductivity of NW sample 3 were also measured using a four-probe measurement procedure for most of the temperature range. In this new procedure discussed in detail elsewhere,[20] the NW itself was used as a differential thermocouple to measure the temperature drops at the two contacts between the NW and the two membranes, so that both the contact thermal

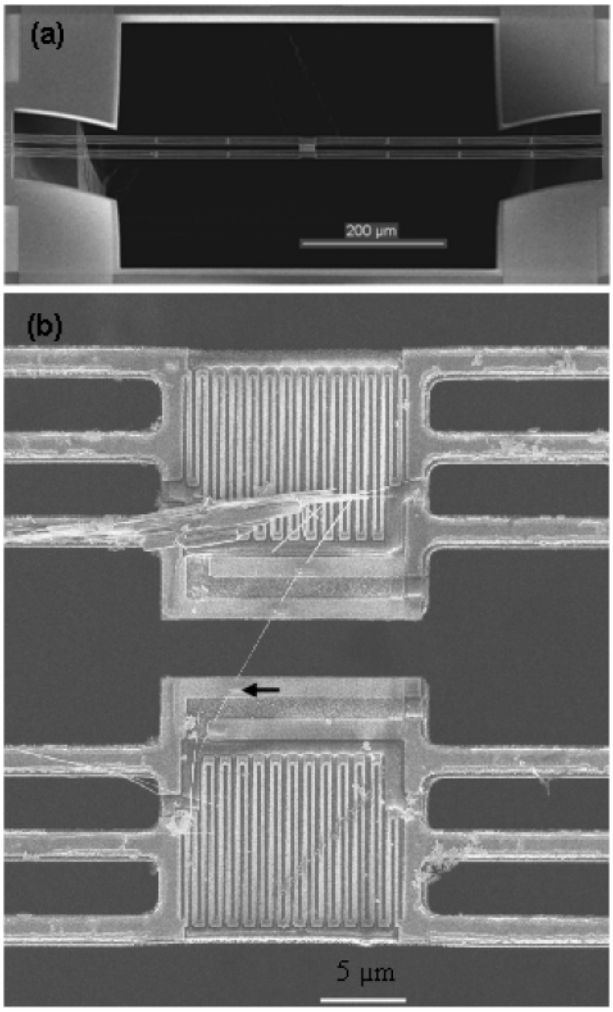

Figure 1. (a) SEM image of the suspended device. (b) SEM image of the two central membranes of the device showing a $CrSi_2$ NW (sample 1) trapped between the two membranes. The arrow points to one of the four Pt patterns deposited on the NW with FIB.

resistance and the intrinsic thermal resistance of the NW can be determined and the thermal conductivity can be calculated from the intrinsic thermal resistance. Except at temperature $T = 120$ and 200 K for NW 1, the contact thermal resistance was not measured for NWs 1 and 2. In this case, the total thermal conductivity (κ_{total}) was calculated from the total thermal resistance (R_{total}) of the sample including the contact thermal resistance, i.e., $\kappa_{total} = L/AR_{total}$, where *A* is the cross section area and *L* is the length of the suspended segment of the NW.

Upon completion of the TE measurements, the crystal structure of the measured NW was characterized using TEM. The diameter (*d*) was measured with TEM to be 78, 97, and 103 nm for NWs 1, 2, and 3, respectively. The lengths of the suspended segment of the NW were 5.8, 2.8, and 4.0 μm for NW 1, 2 and 3, respectively. The high-resolution TEM (HRTEM) image (Figure 2b) of NW 2 shows lattice resolved fringes as expected for the hexagonal structure (space group $P6_222$) of $CrSi_2$ NW. From the HRTEM image and the corresponding fast Fourier transform (FFT) pattern (Figure 2c), the growth direction of this NW was determined to be along the *c*-axis, i.e., the ⟨0001⟩ direction. The growth

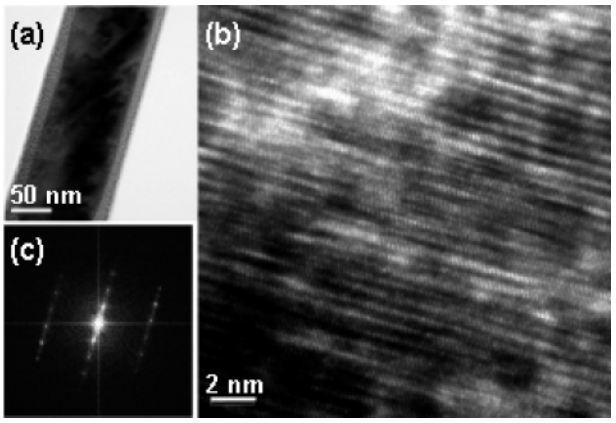

Figure 2. (a) Low-magnification TEM image of NW sample 2. (b) HRTEM image of the same NW and (c) the corresponding FFT pattern.

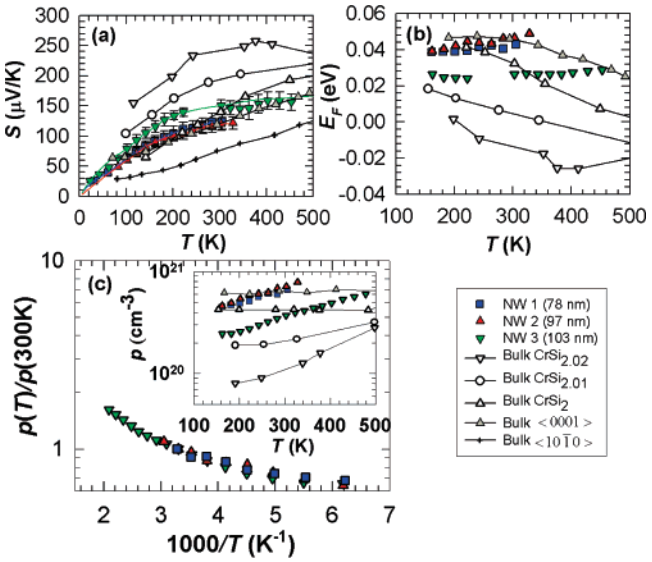

Figure 3. (a) Seebeck coefficient (S) as a function of temperature (T) for three $CrSi_2$ NWs, bulk $CrSi_2$, $CrSi_{2.01}$, and $CrSi_{2.02}$ reported by Shinoda et al. in ref 21, and bulk crystals along the ⟨0001⟩ and ⟨10$\bar{1}$0⟩ directions reported by Nishida in ref 17. The blue, red, and green lines in (a) are calculation results that were made to fit the measured Seebeck coefficient of NWs 1, 2, and 3, respectively. (b) Fermi energy (E_F) of the NW and bulk samples as a function of T. (c) Hole concentration (p) normalized by p at 300 K as a function of 1000/T for the three NWs. Inset: p as a function of T for the NW and bulk samples.

directions of the other two NWs were also found to be along the ⟨0001⟩ direction, consistent with the observation of all as-grown $CrSi_2$ NWs.[15]

Figure 3a shows the measurement results of S versus T for the three NWs together with those reported by Shinoda et al.[21] and Nishida[17] for bulk $CrSi_2$ crystals. It was found that the two-probe Seebeck coefficient measured using the two inner Pt electrodes was smaller by less than 2% than the four-probe S determined by the procedure in ref 20. Shinoda et al. examined the effect of Si doping on the TE properties of bulk crystals with varying compositions including $CrSi_2$, $CrSi_{2.01}$, and $CrSi_{2.02}$. These samples of different Si concentrations were all found to be degenerate p type semiconductors, and excess Si concentration was found to act as donors. The crystal direction for the reported properties was not specified in their work. Nishida reported anisotropic TE properties of bulk $CrSi_2$ in the directions parallel and perpendicular to the c-axis corresponding to the ⟨0001⟩ and ⟨10$\bar{1}$0⟩ directions, respectively. Shinoda et al.'s results for $CrSi_2$ are close to Nishida's results along the ⟨0001⟩ direction. The three $CrSi_2$ NWs measured in this work exhibit a positive Seebeck coefficient that is comparable to Nishida's results along the ⟨0001⟩ direction, which is exactly the NW growth direction determined by TEM. This comparison underscores the importance of determining the growth direction of the NW for which the TE properties were measured. The three NWs were from two different batches of samples that were synthesized at different times. NWs 1 and 2 were from the same batch. The Seebeck coefficient values of these two samples were almost identical and close to Nishida's results for the ⟨0001⟩ direction and Shinoda et al.'s results for $CrSi_2$ at $T < 300$ K. NW sample 3 from a different batch shows a higher Seebeck coefficient than NW 1 and NW 2.

Seebeck coefficient measurements offer a powerful method to probe E_F and thus majority carrier type and concentration based on the sensitive dependence of S on E_F. In fact, connecting a hot probe to a semiconductor and measuring the sign of the generated thermovoltage is a textbook example of how to determine the majority carrier type. However, this powerful method has not been fully utilized for elucidating the electronic structure of nanostructured electronic and TE materials except for very few studies such as one on semiconductor junctions.[22] Here, we have calculated the E_F of the three NWs from the measured Seebeck coefficient using both a single band model and a two band model. As found by Shinoda et al.,[21] $CrSi_2$ is a highly degenerate p-type semiconductor and the hole mobility is about 100 times higher than the electron mobility. Hence, the two-band model was found to yield the same result as the following single valence band model for both the bulk $CrSi_2$ crystals and the NWs studied here

$$S = \frac{k_B}{e}\left\{\frac{(r_p + 5/2)F_{r_p+3/2}(\eta)}{(r_p + 3/2)F_{r_p+1/2}(\eta)} - \eta\right\} \qquad (1)$$

$$\eta = \frac{E_F}{k_B T}$$

In eq 1, k_B is Boltzmann's constant, e is electron charge, E_F is the Fermi energy measured from the valence band edge (E_v) and increases when it moves down into the valence band, and $F_r(\eta)$ is the Fermi−Dirac integral

$$F_r(\eta) = \int_0^\infty \frac{\zeta^r}{\exp(\zeta - \eta) + 1}\, d\zeta \qquad (2)$$

Besides E_F, the Seebeck coefficient also depends on the exponent (r_p) in the energy (E) dependence of the hole relaxation time (τ_p), i.e., $\tau_p = \tau_0 E^{r_p}$, where τ_0 and r_p are two constants. The parameter r_p takes a value of −0.5 when the mobility is limited by either acoustic phonon scattering[21,23] or boundary scattering[24] and a value of 0.5 when impurity

scattering is dominant.[23] At temperatures above 150 K, acoustic phonon scattering was found to be the dominant carrier scattering mechanism for $CrSi_2$ bulk crystals[17,21] and also for the NWs here, as discussed in the following. Hence, $r_p = -0.5$ is appropriate for $T > 150$ K. For $T < 150$ K, impurity scattering could become increasingly important so that r_p could increase with decreasing temperature and cannot be determined accurately. Therefore, we have used $r_p = -0.5$ to analyze only the measurement data for $T > 150$ K, which is the temperature range relevant to practical thermoelectric applications.

The reduced Fermi energy η in eq 1 was adjusted to match the calculated S value with the experimental result at each temperature. The obtained E_F is shown in Figure 3b as a function of temperature for the NWs and the bulk crystals reported in the literature. The results reveal that the $CrSi_2$ NWs were degenerate p-type semiconductors just like the corresponding bulk crystals.

The obtained E_F was further used to calculate the hole concentration. The hole effective mass in bulk $CrSi_2$ samples was determined experimentally to be $m_p = 5m_0$,[17,21] where m_0 is the electron rest mass. Because of the large effective mass, the energy separation of two adjacent hole subbands in the NW, i.e., $\Delta E \approx 3(\pi^2\hbar^2)/2m_pd^2$, is comparable to thermal energy at temperatures below 1 K. Hence, for the studied NWs with relatively large diameters, there exists little quantum confinement effect that could modify the band structure, density of states, and effective mass in the NW. Thus, the hole concentration (p) can be calculated using the bulk band parameters according to the following

$$p = \frac{(2m_p^* k_B T)^{3/2}}{2\pi^2\hbar^3} F_{1/2}(\eta) \qquad (3)$$

For Shinoda et al.'s bulk crystals of varying compositions,[21] E_F decreases, i.e., moves toward the mid gap, with increasing Si concentration. Moreover, the inset of Figure 3c shows that as the Si concentration increases from $CrSi_2$ to $CrSi_{2.02}$, the hole concentration decreases. Hence, excess Si atoms act as donors and Cr atoms act as acceptors in the degenerate p-type crystals. Additionally, the E_F in Shinoda et al.'s bulk crystals decreases with increasing temperature because of thermal activation of electrons from the valence band to the conduction band. The E_F of Nishida's bulk sample is higher than those for Shinoda et al.'s samples, indicating higher Cr acceptor concentration in Nishida's bulk sample. For Nishida's sample, E_F is approximately constant between 150 and 250 K, suggesting that the acceptors were not yet fully activated because of the higher acceptor concentration, and decreases with increasing temperature for $T > 300$ K because of thermally generated intrinsic carriers. The obtained E_F of the NWs is approximately constant over the temperature range. Moreover, the hole concentrations in the NWs increase more rapidly with temperature than those in the bulk crystals.

To better understand the observed E_F and hole concentrations in the NWs, we have plotted the $p(T)/p(300\ K)$ ratio versus $1000/T$ for the three NWs. As shown in Figure 3c, the obtained curves nearly collapsed into a single curve for the three NWs at $1000/T$ between 3.3 and 6.6 corresponding to temperatures from 150 to 300 K. The approximately linear behavior of the curves indicates a thermally activated conduction process. The thermal activation energy was estimated from the slope to be 0.013 eV. This small activation energy appears to represent acceptor ionization energy and was similar to the corresponding values of 0.01 and 0.019 eV, respectively, observed in $CrSi_2$ films.[25,26] Similar shallow doping levels in bulk silicides were reported in refs 27 and 28.

It has been reported that the extrinsic to intrinsic transition temperature in bulk single-crystal $CrSi_2$ is about 600 K.[28] Hence, it is reasonable to find that the $CrSi_2$ NWs in our measurement are still within the extrinsic region in the measurement temperature ranges. At temperature between 150 and 450 K where the thermal energy is comparable to the acceptor ionization energy, more acceptors were ionized at higher temperatures, increasing the hole concentration with temperature. The acceptor concentrations in the NWs could have been higher than those in the bulk crystals, so that the hole concentration increased more rapidly with temperature in the NWs than in the bulk crystals. Because of the high acceptor concentrations in the NWs, the acceptors were not fully ionized at temperatures up to 450 K, resulting in the approximately constant E_F. Because NW 3 was found to have lower hole concentration than NWs 1 and 2, we can further infer that NW 3 had slightly lower Cr acceptor concentration or higher Si donor concentration than NWs 1 and 2.

Figure 4a shows the measured σ versus T results for the three NWs together with the bulk values reported in the literature. The electrical conductivity of the NWs shows much weaker temperature dependence than those of the bulk crystals. NW 1 and NW 2 are from the same batch and show the same trend although their actual values are slightly different. NW 3 shows a lower electrical conductivity than the other two NWs. In addition, the electrical conductivities for NW 1 and NW2 increase slightly with temperature, whereas the electrical conductivity of NW 3 decreases slightly with increasing temperature for $T > 200$ K.

To understand the observed electrical conductivity, we have further used the calculated hole concentration and the measured electrical conductivity to obtain the carrier mobility (μ) based on the relation $\sigma = pe\mu$. Figure 4b shows the temperature dependence of the carrier mobility of the NWs and bulk crystals. The NW mobility values and temperature dependence are very close to the bulk values along the $\langle 0001 \rangle$ direction obtained by Nishida. Because the mobility obtained on the NWs is similar to that of the bulk crystal in the same crystal direction, boundary scattering was not the dominant carrier scattering mechanism in the NWs. The decreasing mobility with temperature also suggests that acoustic phonon scattering instead of boundary scattering determined the hole mobility for $T > 150$ K, just like the bulk crystals.[17,21]

Figure 4b shows that the mobilities of the Nishida's bulk sample in the $\langle 0001 \rangle$ direction and the NWs are lower than those for Shinoda's bulk samples, for which the crystal direction was not specified. Note that the mobility in the $\langle 10\bar{1}0 \rangle$ direction is higher than that in the $\langle 0001 \rangle$ direction. In addition, the bulk mobilities decrease with increasing Si concentration at $T > 200$ K.

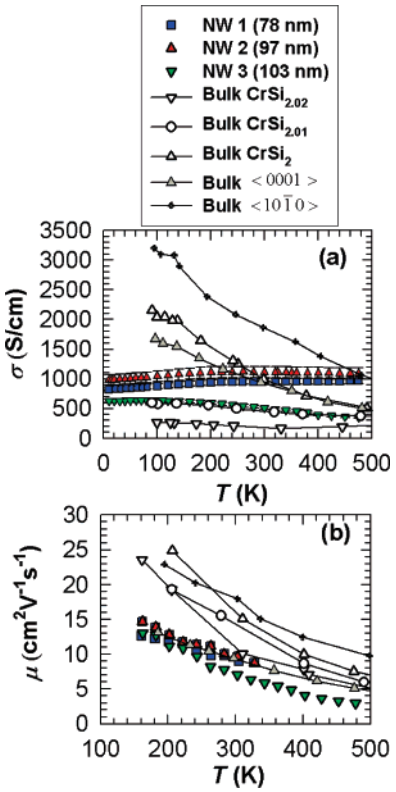

Figure 4. (a) Electrical conductivity (σ) and (b) hole mobility (μ) as a function of temperature for three $CrSi_2$ NWs, bulk $CrSi_2$, $CrSi_{2.01}$, and $CrSi_{2.02}$ reported by Shinoda et al. in ref 21, and bulk crystals in $\langle 0001 \rangle$ and $\langle 10\bar{1}0 \rangle$ directions reported by Nishida in ref 17.

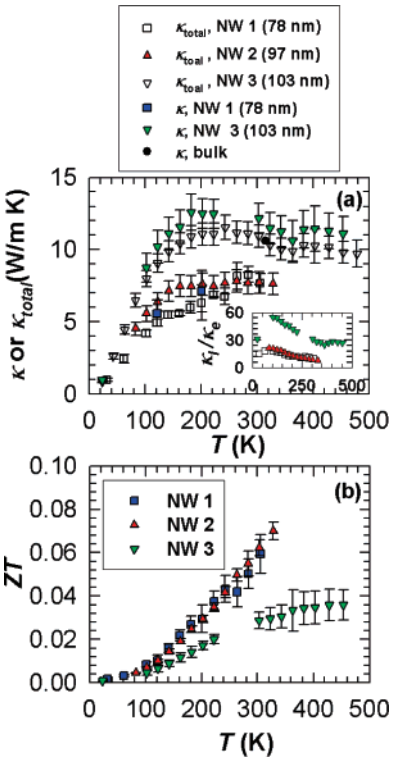

Figure 5. (a) κ or κ_{total} as a function of temperature for three $CrSi_2$ NWs and bulk $CrSi_2$ from ref 34. The inset shows the κ_l/κ_e ratio for NW sample 1 (unfilled squares), 2 (red up triangles), and 3 (green down triangles). (b) ZT as a function of temperature for the three $CrSi_2$ NWs. For the ZT calculation, κ was used for NW 3 and κ_{total} was used for NWs 1 and 2.

The inset of Figure 3c reveals that NW 3 has lower hole concentration, most probably because of a lower Cr acceptor or higher Si donor concentration than NW 1 and 2. The mobility of NW 3 is close to those of NWs 1 and 2 at $T <$ 200 K and becomes slightly lower than those of the other two NWs at $T >$ 200 K. This difference is consistent with the observed bulk behavior of decreasing mobility with increasing Si concentration at $T >$ 200 K. The slightly lower mobility of NW 3 at $T >$ 200 K could have caused the slightly decreasing electrical conductivity with temperature at $T >$ 200 K. Nevertheless, the temperature dependence of the electrical conductivity was rather weak for all three NWs. The weak temperature dependence in the NWs is attributed to the competition between decreasing hole mobility with temperature and rapidly increasing hole concentration with temperature as a result of high acceptor concentrations in the NWs.

It is worth noting that the bulk mobility results were obtained from Hall measurement. However, it is impossible to perform Hall measurement on NWs due to its peculiar 1-D geometric configuration. It has been an active pursuit to develop experimental methods to obtain the carrier concentration and mobility in NWs.[4−6,29−31] On the basis of the above analysis, combined Seebeck coefficient and electrical conductivity measurements on NWs can be used to assess the carrier concentration and mobility in NWs. The advantage of this approach over the SdH method[4] is that the current approach can be used for both degenerate and nondegenerate NWs while the SdH method is not applicable for degenerately doped NWs. In addition, we note that transport characteristics have been used to estimate the carrier mobility in carbon nanotube (CNT) transistors.[32,33] However, the accuracy of this method is limited by the uncertainties in the extracted threshold voltage and in the calculation of the capacitance of the complex nanotube-gate geometry. For degenerate NWs with the diameter 1 or more orders of magnitude larger than a CNT, moreover, the threshold voltage can be very high, making it difficult to measure or extract the threshold voltage accurately.

In addition to the Seebeck coefficient and electrical conductivity, the thermal conductivity of the NWs was also measured. Figure 5a shows the measured thermal conductivity as a function of temperature for the three NWs. It was found that κ_{total} was smaller by less than about 10% than the four-probe κ determined using the procedure in ref 20. It is worth noting that we exclude the native oxide layer (usually about 10 nm thick) when determining the NW diameter for both σ and κ calculations. This may cause some errors in the calculated κ, but the effect should be small because the thermal conductivity of the amorphous oxide is expected to be much smaller than the single-crystal $CrSi_2$ core of the NW. The inset to Figure 5a shows the κ_l/κ_e ratio that was calculated from the measured electrical conductivity and thermal conductivity results based on the Wiedemann−Franz law. This ratio is much larger than unity, so that phonons dominate heat conduction in the NWs. The thermal conductivity increases with temperature until at about 200 K, at which point the thermal conductivity reaches a plateau and

subsequently starts to decrease with increasing T. Near room temperature, the thermal conductivities of three NWs are almost the same as the bulk value reported in the literature.[34] This finding suggests that the Umklapp scattering is still the dominant phonon scattering process in the three NWs at room temperature. We could not find low-temperature thermal conductivity data for bulk $CrSi_2$ crystals in the literature. It is likely that the thermal conductivity of the NWs was reduced below the bulk values by diffuse phonon−surface scattering at low temperatures. Figure 5a shows that κ_{total} decreases slightly with decreasing NW diameter at temperature below 300 K, likely due to decreased phonon−surface scattering mean free path with decreasing diameter.

Because the three transport properties that enter into ZT can all be obtained by this measurement method on the same NW sample, the ZT value of the NW can be readily obtained from the measurement results. As shown in Figure 5b, NWs 1 and 2 from the same batch show nearly the same ZT values, which are higher than those of NW 3 from a different batch. The difference can be attributed to mainly the different acceptor concentrations in the two different batches of NWs. Hence, it is necessary to further refine the synthesis method in order to control and tune the doping concentration as well as the NW diameter so as to maximize the ZT of the $CrSi_2$ NWs.

Nevertheless, ZT enhancement was not expected in the three $CrSi_2$ NWs because electrons and phonons were not confined in the NWs. The large hole effective mass in $CrSi_2$ prevents quantum confinement of holes unless for extremely low temperatures or extremely small diameters. Using thermal conductivity expression $\kappa = Cvl/3$, where C, v, and l are specific heat, sound velocity, and phonon mean free path, we estimate that l is lower than 10 nm in $ReSi_{1.75}$ at room temperature. Being in the same silicide family, $CrSi_2$ is expected to have a similar short l value, which is much smaller than the diameter of the three NWs. Consequently, the thermal conductivity reduction was found to be small in these NWs at room temperature.

This experiment demonstrates that the thermoelectric property−crystal structure relationship of individual NWs can be established by the measurement method that is capable of characterizing the thermoelectric properties and crystal structure on the same individual NW. We show that combined Seebeck coefficient and electrical conductivity measurements provide an effective approach to probing the Fermi Level, carrier concentration, and mobility in NWs, especially at near room temperature and above that are relevant for most device applications. The obtained Seebeck coefficient and hole mobility of the NWs are close to those reported for bulk single crystals. The low-temperature measurement results also reveal increased phonon−surface scattering with decreased NW diameter. The general NW growth method and the characterization technique reported here can be applied to verify ZT enhancement in other NW systems with small effective mass or large phonon mean free path.

Acknowledgment. The authors at UT acknowledge funding support from Office of Naval Research Contract N00014-04-1-0532 (Program manager: Dr. Mihal Gross) and National Science Foundation Award CBET 0239179. One of the authors (M.T.P.) is supported by a NSF Graduate Research Fellowship. The authors at UW thank NSF (CAREER DMR-0548232), 3M Nontenured Faculty Award, and DuPont Young Professor Grant for financial support. We thank Dr. X. X. Gao for help with HRTEM.

References

(1) Harman, T. C.; Taylor, P. J.; Walsh, M. P.; LaForge, B. E. *Science* **2002**, *297*, 2229.
(2) Venkatasubramanian, R.; Siivola, E.; Colpitts, T.; O'Quinn, B. *Nature* **2001**, *413*, 597.
(3) Hsu, K. F.; Loo, S.; Guo, F.; Chen, W.; Dyck, J. S.; Uher, C.; Hogan, T.; Polychroniadis, E. K.; Kanatzidis, M. G. *Science* **2004**, *303*, 818.
(4) Heremans, J.; Thrush, C. M. *Phys. Rev. B* **1999**, *59*, 12579.
(5) Lin, Y. M.; Cronin, S. B.; Ying, J. Y.; Dresselhaus, M. S.; Heremans, J. P. *Appl. Phys. Lett.* **2000**, *76*, 3944.
(6) Lin, Y. M.; Dresselhaus, M. S. *Appl. Phys. Lett.* **2003**, *83*, 3567.
(7) Borisenko, V. E. *Semiconducting Silicides*; Springer: Berlin, 2000; Vol. 39.
(8) Rowe, D. M. *CRC Handbook of Thermoelectrics*; CRC Press: Boca Raton, FL, 1994; Chapters 23−25.
(9) Sakamaki, Y.; Kuwabara, K.; Gu, J.; Inui, H.; Yamaguchi, M.; Yamamoto, A.; Obara, H. *Mater. Sci. Forum* **2003**, *426−432*, 1777.
(10) Wu, Y.; Xiang, J.; Yang, C.; Lu, W.; Lieber, C. M. *Nature* **2004**, *430*, 61.
(11) Ouyang, L.; Thrall, E. S.; Deshmukh, M. M.; Park, H. *Adv. Mater.* **2006**, *18*, 1437.
(12) Schmitt, A. L.; Bierman, M. J.; Schmeisser, D.; Himpsel, F. J.; Jin, S. *Nano Lett.* **2006**, *6*, 1617.
(13) Schmitt, A. L.; Zhu, L.; Schmeisser, D.; Himpsel, F. J.; Jin, S. *J. Phys. Chem. B* **2006**, *110*, 18142.
(14) Song, Y.; Schmitt, A. L.; Jin, S. *Nano Lett.* **2007**, *7*, 965.
(15) Szczech, J. R.; Schmitt, A. L.; Bierman, M. J.; Jin, S. Single-Crystal Semiconducting Chromium Disilicide Nanowires Synthesized via Chemical Vapor Transport. *Chem. Mater.*, in press.
(16) Boren, B. *Ark. Kemi. Mineral. Geol.* **1933**, *11A* (10), 1.
(17) Nishida, I. *J. Mater. Sci.* **1972**, *7*, 1119.
(18) Shi, L.; Li, D.; Yu, C.; Jang, W.; Kim, D.; Yao, Z.; Kim, P.; Majumdar, A. *J. Heat Transfer* **2003**, *125*, 881.
(19) Yu, C. H.; Saha, S.; Zhou, J.; Shi, L.; Cassell, A. M.; Cruden, B. A.; Ngo, Q.; Li, J. *J. Heat Transfer* **2006**, *128*, 234.
(20) Mavrokefalos, A.; Pettes, M. T.; Zhou, F.; Shi, L. *Rev. Sci. Instrum.* **2007**, *78*, 34901.
(21) Shinoda, D.; Asanabe, S.; Sasaki, Y. *J. Phys. Soc. Jpn.* **1964**, *19* (3), 269.
(22) Lyeo, H. K.; Khajetoorians, A. A.; Shi, L.; Pipe, K. P.; Ram, R. J.; Shakouri, A.; Shih, C. K. *Science* **2004**, *303*, 816.
(23) Ziman, J. M. *Electrons and Phonons*; Clarendon: Oxford, 1960.
(24) Seol, J. H.; Moore, A. L.; Saha, S. K.; Zhou, F.; Shi, L.; Ye, Q. L.; Scheffler, R.; Mingo, N.; Yamada, T. *J. Appl. Phys.* **2007**, *101*, 23706.
(25) Galkin, N. G.; Velitchko, T. V.; Skripka, S. V.; Khrustalev, A. B. *Thin Solid Films* **1996**, *280*, 211.
(26) Nava, F.; Tien, T.; Tu, K. N. *J. Appl. Phys.* **1985**, *57* (6), 2018.
(27) Imai, M.; Hirano, T. *J. Alloys Compd.* **1995**, *224* (1), 111.
(28) Nishida, I.; Sakata, T. *J. Phys. Chem. Solids* **1978**, *39* (5), 499.
(29) Zhang, Z. B.; Sun, X. Z.; Dresselhaus, M. S.; Ying, J. Y.; Heremans, J. P. *Appl. Phys. Lett.* **1998**, *73*, 1589.
(30) Hong, K. M.; Yang, F. Y.; Liu, K.; Reich, D. H.; Searson, P. C.; Chien, C. L.; Balakirev, F. F.; Boebinger, G. S. *J. Appl. Phys.* **1999**, *85*, 6184.
(31) Gu, Y.; Romankiewicz, J. P.; David, J. K.; Lensch, J. L.; Lauhon, L. J. *Nano Lett.* **2006**, *6*, 948.
(32) Martel, R.; Schmidt, T.; Shea, H. R.; Hertel, T.; Avouris, P. *Appl. Phys. Lett.* **1998**, *73*, 2447.
(33) Durkop, T.; Getty, S. A.; Cobas, E.; Fuhrer, M. S. *Nano Lett.* **2004**, *4*, 35.
(34) Neshpor, V. S. *J. Eng. Phys.* **1968**, *15* (2), 750.

NL0706143